Hindawi Publishing Corporation
Journal of Nanomaterials
Volume 2011, Article ID 830157, 8 pages
doi:10.1155/2011/830157

Research Article

Diameter- and Shape-Controlled ZnS/Si Nanocables and Si Nanotubes for SERS and Photocatalytic Applications

Xue Chen,[1,2,3] Chun-Sing Lee,[2] Xiangmin Meng,[1] and Wenjun Zhang[1,2]

[1] *Key Laboratory of Photochemical Conversion and Optoelectronic Materials, Technical Institute of Physics and Chemistry, Chinese Academy of Sciences, Beijing 100190, China*
[2] *Department of Physics and Materials Science, Center Of Super-Diamond and Advanced Films (COSDAF), City University of Hong Kong, Hong Kong*
[3] *Graduate School of Chinese Academy of Sciences, Beijing 100039, China*

Correspondence should be addressed to Xiangmin Meng, xmmeng@mail.ipc.ac.cn and Wenjun Zhang, apwjzh@cityu.edu.hk

Received 21 December 2010; Accepted 26 April 2011

Academic Editor: Sherine Obare

ZnS/Si nanocables were synthesized via a simple two-step thermal evaporation method. The shape and diameter of the ZnS/Si nanocables can be controlled by adjusting the morphologies of the ZnS nanostructures (nanowire or nanoribbon) obtained in the first step and the deposition time of the Si shell in the second step, respectively. Furthermore, we obtained polycrystalline Si nanotubes with different shapes and diameters by etching away the inner ZnS core. The as-prepared Si nanotubes were employed as SERS-active substrates, which exhibited a high sensitivity for the detection of R6G. The Si nanotubes also showed effective photocatalytic activity on the decomposition of R6G under the irradiation of visible light.

1. Introduction

Over the past decade, one-dimensional heterostructures have attracted particular interest due to their unique properties and potential applications in nanoelectronics and nanophotonics [1–5]. Among all these heterostructures, the radial nanocable structures have advantages because of its higher efficient injection current in comparison with the axial structures [6–8]. In particular, Si-based heterostructures are of special interest due to the important role of Si in the modern microelectronics industry. To meet the increasing demands of various applications, different methods have been developed for the fabrication of Si-based nanomaterials, such as the laser-ablation metal-catalytic method [9], chemical vapor deposition [10], chemical etching method [11], and solution growth [12]. To date, several Si-based core/shell heterostructures, such as Ge/Si [13, 14], Si/SiO_2 [15], Si/SiOx [16], ZnS/Si [17], ZnSe/Si [18], Ag/Si [19], have been fabricated using different growth processes. Since the properties of nanomaterials greatly depend on their structures, shapes, sizes, and chemical compositions [20–23], the crystalline semiconductor nanocables with controllable structures, shapes, diameters, and chemical compositions would have new applications in many areas, such as photocatalysis, biological and chemical sensing, and nanooptoelectronics.

In this paper, we report a simple thermal evaporation approach for the synthesis of shape- and diameter-controlled Si-based nanocables. Furthermore, polycrystalline Si nanotubes with different shapes and diameters were obtained by etching away the inner ZnS core. Owing to the large specific surface areas, the Si nanotubes would have advantageous applications in biological, chemical, and electrical devices. Here, the Si nanotubes were used as the surface-enhanced Raman spectroscopy (SERS)-active substrates for the ultrasensitive molecule detection and the photocatalyst for organic dyes degradation. The results indicate that the Si nanotubes might be a promising material for sensing and photocatalytic applications.

2. Experimental Section

2.1. The Synthesis of ZnS Nanowires and Nanoribbons. ZnS nanowires and nanoribbons were first synthesized via typical

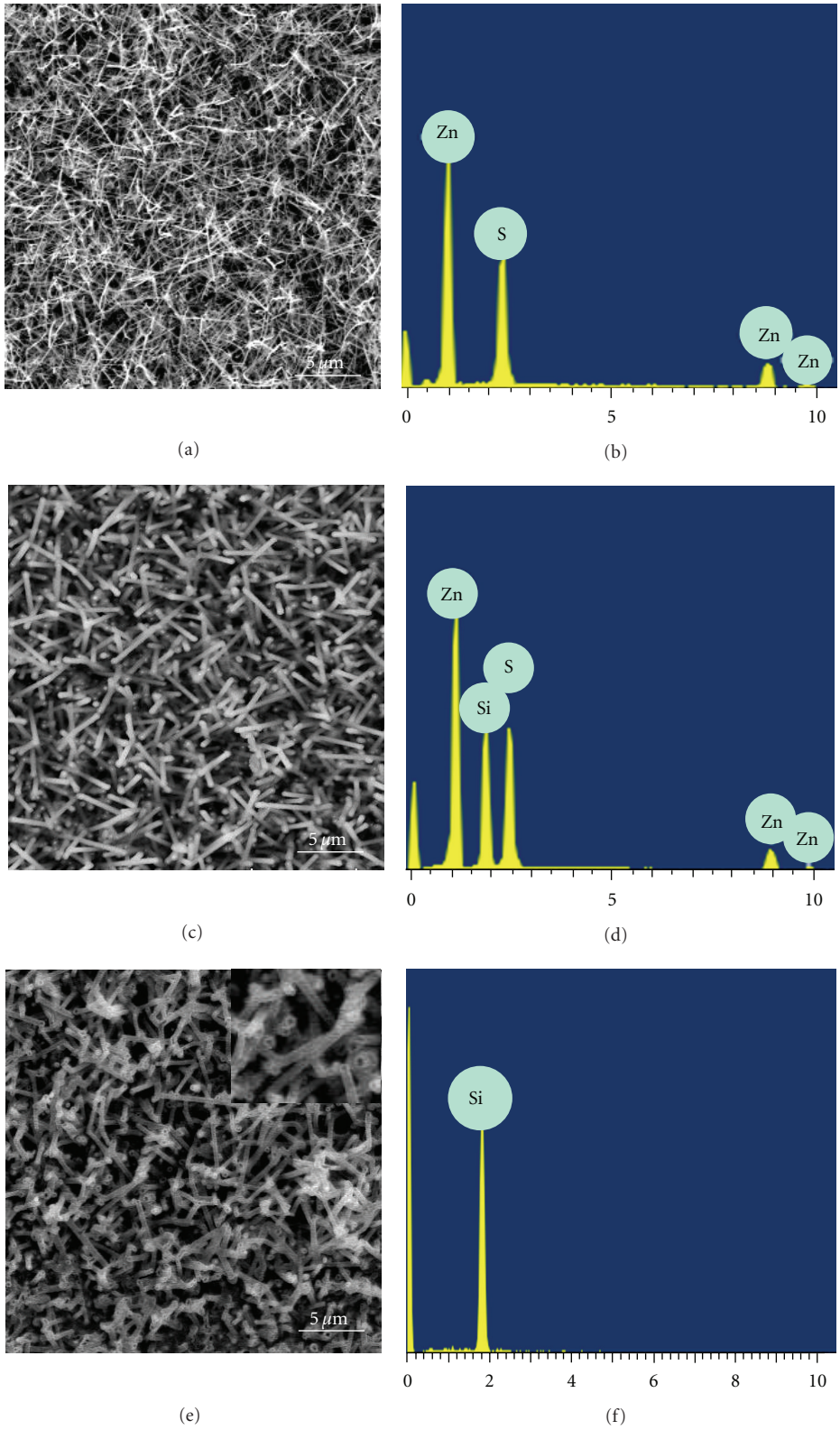

Figure 1: (a) and (b) An SEM image and EDS spectrum of the ZnS nanowires obtained after the first deposition step; (c) and (d) an SEM image and EDS spectrum of the ZnS/Si nanocables after deposition of Si onto the ZnS nanowires; (e) and (f) an SEM image and EDS spectrum of the Si nanotubes obtained by chemical etching of the sample in Figure 1(c); Inset in Figure 1(e), an enlarged SEM image showing the open-ended tubular structures.

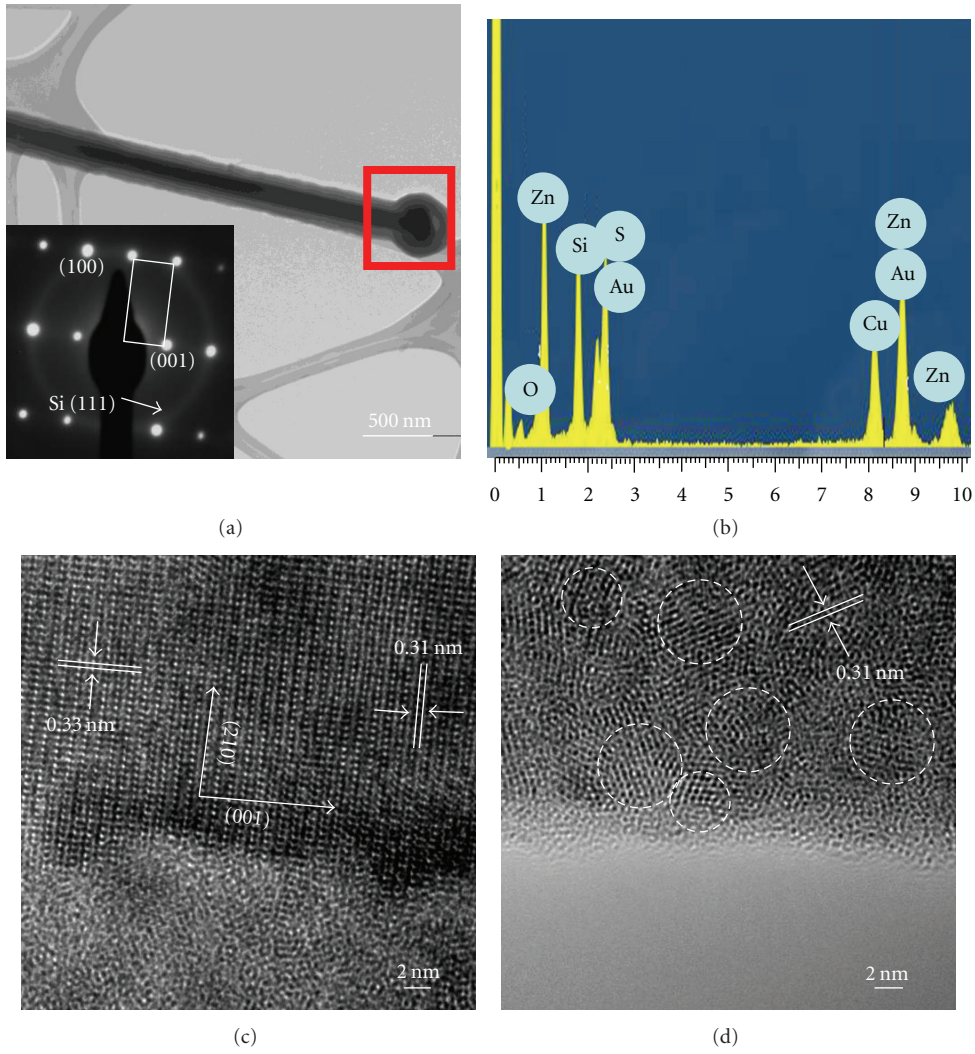

FIGURE 2: (a) A TEM bright field image of a ZnS/Si nanocable showing a clear core-shell structures (inset is an SAED pattern of the nanocable); (b) an EDS spectrum of the cable; (c) a high-resolution TEM image of the inner core ZnS; and (d) a high-resolution TEM image of the polycrystalline sheath Si.

chemical vapor deposition (CVD) method [24, 25]. In a typical experiment, 1 g of ZnS powder (Alfa Aldrich, 99.99%) as the source material was placed at the center of a quartz tube. Several pieces of Si wafers (1 cm × 2 cm) coated with 5 nm-thick gold films were used as substrates and placed at about 9 cm downstream of the ZnS powder. The quartz tube was placed in a tube furnace and was evacuated to a pressure of 4.5×10^{-4} Torr. A carrier gas of high-purity argon premixed with 5% H_2 was continuously fed into the tube at a flow rate of 25 standard cubic centimeters per minute (sccm) and a pressure of 100 Torr throughout the whole experiment. Temperature at the center of the tube was ramped up at 20°C/min to reach a temperature of 1050°C and kept at this temperature for 2 hours. Temperatures at the silicon substrates were measured to range from 600 to 800°C. After the furnace was naturally cooled down to room temperature, ZnS nanowires and nanoribbons were deposited in the temperature region of about 600°C and 800°C, respectively, on the Si wafers.

2.2. The Synthesis of ZnS/Si Nanocables. The experiment was then repeated by replacing the ZnS powder with SiO powder (Alfa Aldrich, 99.99%) and adjusting some of the experimental parameters. The as-prepared ZnS nanowires or nanoribbons were placed 7 cm down stream of the SiO powder. High-purity argon with 5% H_2 gas was fed at 50 sccm and a pressure of 300 Torr. Center of the tube was heated to 1350°C and held for 30 minutes before cooling.

2.3. Materials Characterization. Compositions, morphologies, and microstructures of the prepared samples were characterized with X-ray diffraction (XRD, Philips X'Pert), scanning electron microscopy (SEM, HITACHI s-4300), and transmission electron microscopy (TEM, Philips CM20 and CM200 FEG). SERS was measured using a Renishaw 2000 laser Raman microscope equipped with a 633 nm argon ion laser of 2 μm spot size for excitation. UV-vis absorption spectra were acquired with an Aglient 8453 UV-vis Diode Array Spectrophotometer.

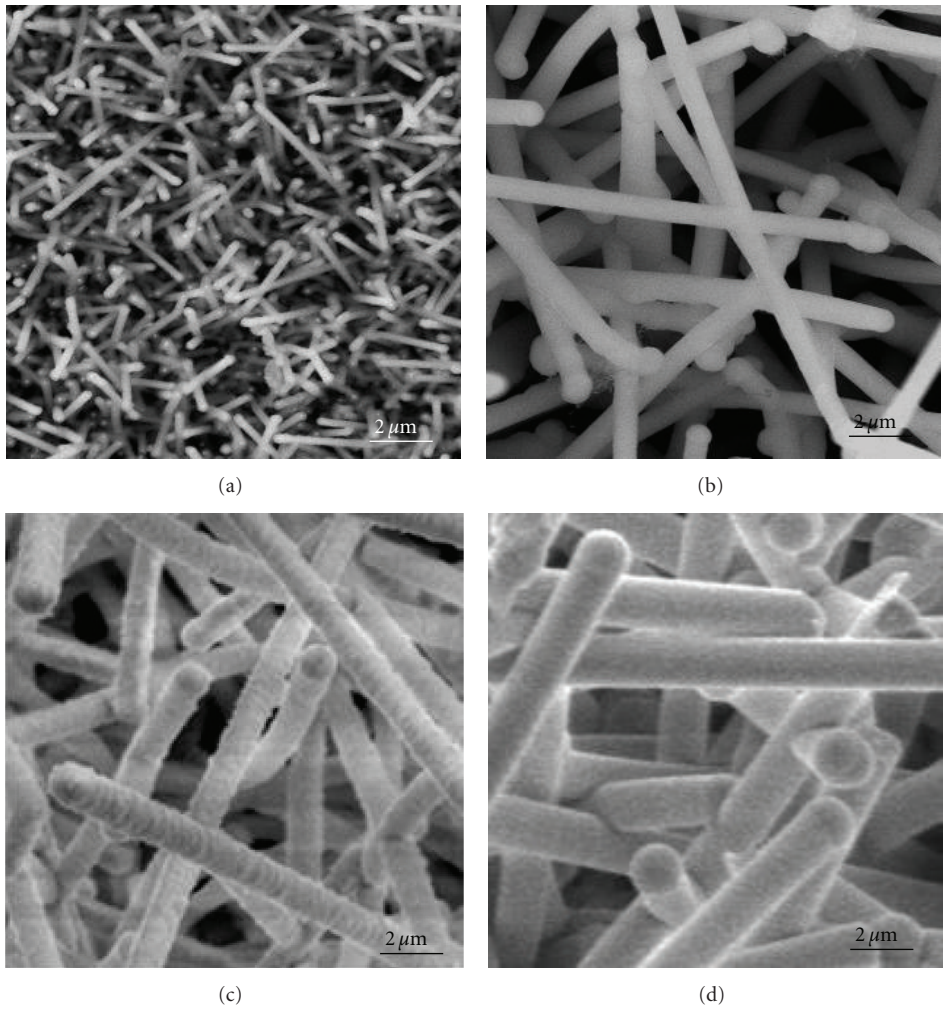

Figure 3: SEM images of ZnS/Si cables with different diameters of (a) 200 nm; (b) 500 nm; (c) 700 nm; (d) 900 nm.

3. Results and Discussion

Figure 1(a) shows an SEM image of the product on the Si substrate after the first deposition step using ZnS powder as source. It consists of a high density of nanowires of about 60 nm in diameter and about 3 μm in length. Using an energy dispersive X-ray spectrometer (EDS) attached to the SEM, the sample is shown to consist of only Zn and S in roughly 1 : 1 atomic ratio (Figure 1(b)). Figure 1(c) shows an SEM image of the sample after the two deposition steps sequentially with ZnS and SiO sources. It can be seen that the morphology of the sample is similar to that shown in Figure 1(a) except that the wires are of larger diameter (about 200 nm). Figure 1(d) shows a typical EDX spectrum of the sample in Figure 1(c). In addition to the Zn and S peaks, an Si peak can be clearly observed. The sample was then immersed in diluted HCl solution for 30 minutes. Figure 1(e) and insert shows that the HCl treatment removes cylindrical core from the wire-like structures in Figure 1(c) and leads to the formation of hallow tubes. Figure 1(f) is the EDS of the sample in Figure 1(e), which only consists of Si.

Structures of the samples shown in Figure 1(c) are further examined with TEM. Figure 2(a) is the TEM image of a typical wire-like structure obtained from the two-step deposition in Figure 1(c) showing that it is a cable with a core/shell structure. The diameter of the inner core is about 60 nm and the thickness of the sheath is around 75 nm. A selected area electron diffraction (SAED) pattern of the cable is shown as an inset in Figure 2(a). The pattern consists of diffraction spots and rings, which can be, respectively, indexed to single-crystalline wurtzite ZnS and polycrystalline Si. Figure 2(b) is an EDS spectrum taken from the tip (as marked by the red box in Figure 2(a)) showing the existence of Zn, S, Si, Au, and a minimal content of O. The Au element comes from the gold nanoparticle at the tip of each ZnS/Si nanocable, which worked as catalyst during the ZnS nanowire growth process.

Figure 2(c) is a high-resolution TEM image of the inner core of a nanocable. Lattice fringes of 0.31 and 0.33 nm correspond well to spacing of the (002) and (100) planes of wurtzite structured ZnS. Figure 2(d) is a high-resolution TEM image showing that the shell region of a typical

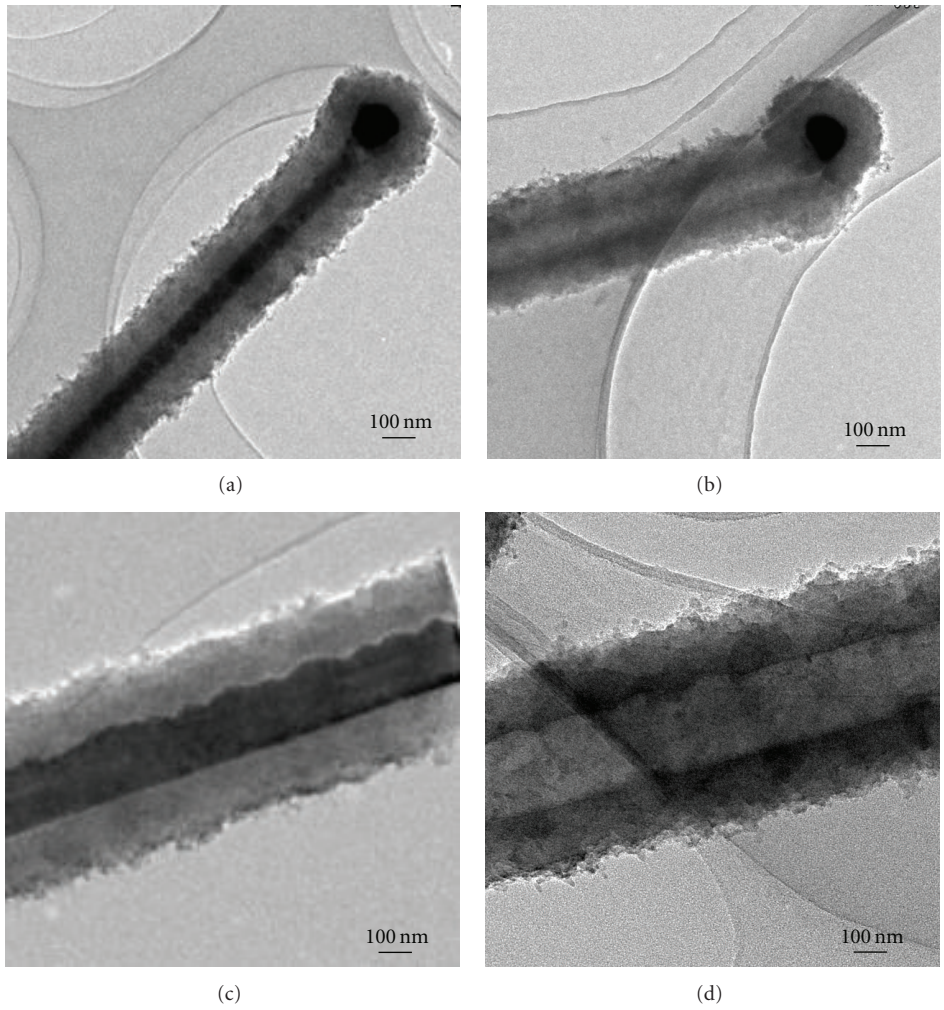

Figure 4: TEM images of ZnS/Si nanocables and Si nanotubes of different shapes: (a) circular cable with ZnS nanowire as template, (b) circular tube, (c) cable of ribbon shape with saw-like ZnS nanoribbon as template, and (d) tube of ribbon shape.

nanocable consisting of many nanocrystallites with a lattice spacing is 0.31 nm which matches well to the (111) spacing of Si. These observations further confirm that the cables have single crystalline cores of wurzite ZnS and shells of polycrystalline Si.

The thickness of Si shell could be easily tuned by adjusting duration of the second deposition step. Figure 3 depicts SEM images of the cables obtained with growing duration of 30 to 120 minutes for the second deposition step. It can be seen that diameter of the cables increases from 200 to 900 nm as the growth duration.

Shape-controllable growth is another important issue in nanoscience and nanotechnology, because some properties would be greatly affected by their shapes. In the experiment, we also found that ZnS nanowires and nanoribbons could be formed in the first deposition step at different temperatures. We found that a ZnS/Si core/shell structure can also be formed with the wire and ribbon shapes (Figures 4(a) and 4(c)). The wire-shaped nanocables in Figure 4(a) have a smooth inner surface and small diameter, in contrast to the ribbon-shaped nanocables (Figure 4(c)) with saw-like ZnS nanoribbons as templates which have a saw-like inner surface and bigger diameter. As mentioned before, the core of the cable can be removed by HCl treatment. It can be seen that a typical cable before HCl etching has a dark-contrasted core of ZnS (Figure 4(a)). After the etching, all the cables show a light-contrasted core (Figure 4(b)). EDS analysis is presented in Figure 1(f), which confirms that there is no longer ZnS in the etched sample. The ZnS core has been etched away leaving the hollow tube of polycrystalline silicon. Similarly ribbon-shaped tubes of polycrystalline Si with saw-like inner surfaces can be formed by etching away the ZnS ribbon cores (Figure 4(d)).

The tubular morphology provides the Si nanostructures with even larger specific surface areas, which might further enhance their performance for applications such as sensors and catalyst. As an example, we investigated the sensing properties of the Si nanotubes as the active substrates for the detection of organic molecules by the SERS technique. As is well known that the Raman signals can be significantly enhanced in the presence of nanometer-sized metallic structures [26] because of the plasmonic resonance between

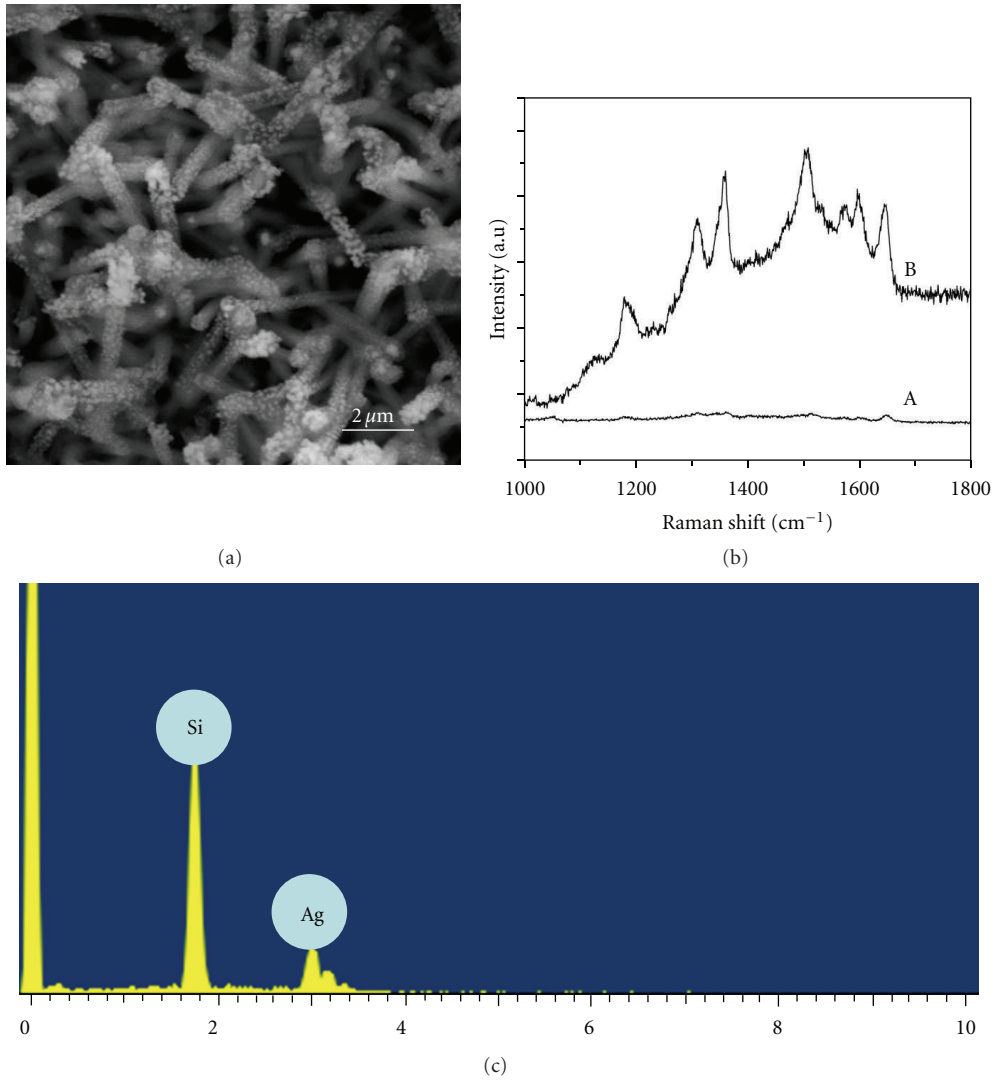

Figure 5: (a) Si nanotubes coated with Ag nanoparticles; (b) SERS spectra of R6G (at the concentration of 1×10^{-8} M) collected on Si wafer (curve A) and Si nanotubes (curve B); (c) The EDX spectroscopy of the samples in Figure 5(a)).

two nearly touching nanoparticles [27]. The uniform dispersion of Ag nanoparticles on Si nanotube surfaces may increase the specific area density of Ag nanoparticles with desired particle-particle spacing and thus improve the SERS sensitivity. In this work, we immersed the as-synthesized Si nanotubes in a solution containing HF (0.5 M) and $AgNO_3$(1×10^{-4} M) for 5 minutes to fabricate the SERS substrates. Ag nanoparticles were uniformly coated on Si nanotubes, as shown in Figure 5(a). The EDX spectroscopy (Figure 5(c)) of the samples reveals that the product consists of Si and Ag. Then two drops of Rhodamine 6G (R6G) (1×10^{-8} M) solution were added. A Raman spectrum from the sample is shown as curve B in Figure 5(b). Curve A is a reference Raman spectrum measured as the same amount of R6G was loaded onto a Si wafer. All the peaks are assigned to the Raman characteristic features of R6G. The peak at 1180 cm^{-1} is assigned to C–C stretching vibration, and peaks at 1310, 1357, 1509, 1575, and 1650 cm^{-1} are associated with the stretching vibration of aromatic C–C [28]. Although the concentration of Rh 6G is very low, the SERS signals of R6G on Si nanotubes can easily be detected and are much stronger than those measured from the Si wafer. Thus, the Si nanotubes synthesized here are very promising substrates for the high-sensitive detection of organic molecules by SERS.

We have also tested the photocatalytic activity of the Si nanotubes. The Si nanotubes were used to degrade Rhodamine 6G (R6G) under the visible lights, and control experiment using Si nanowires were also conducted. Equal amount of the Si nanotubes and Si nanowires of the similar diameters were immersed into 70 mL R6G solutions (1.5×10^{-6} mol/L), respectively, and then irradiated under visible light. After the same time intervals, the Si nanotubes and Si nanowires were taken out, and the absorption spectra of the R6G solutions were recorded. Figure 6 shows the photocatalytic degradation performance of the Si nanotubes and Si nanowires, where C_0 and C are the

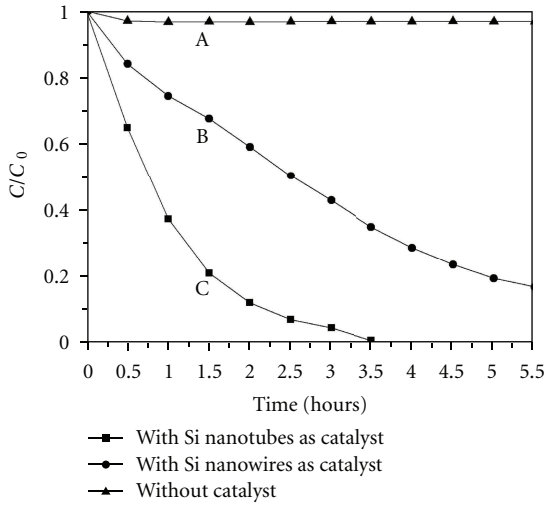

Figure 6: Degradation rate of R6G in solution with Si nanotubes (curve C) and nanowires. (curve B) as catalyst and without catalyst (curve A).

equilibrium concentration of R6G before and after visible light irradiation, respectively. Without catalyst (curve A), no obvious degradation of R6G was observed after irradiation under visible lights for 5.5 hours. In sharp contrast, both Si nanotubes and nanowires accelerated the degradation significantly, and the Si nanotubes (curve C) showed much higher photocatalytic activity than that of nanowires (curve B), which are considered to be due to the larger specific surface areas of the hollow tubular structures.

4. Conclusions

In summary, we demonstrated in this work a simple method to synthesize ZnS/Si nanocables and Si nanotubes with controllable geometries. In this approach, single-crystal ZnS nanowires and nanoribbons grown by CVD were employed as templates for the subsequent CVD growth of polycrystalline Si sheath to form a ZnS/Si core-shell nanocable structure. The ZnS cores were removed by chemical etching to construct Si nanotubes. Diameters and morphologies of the ZnS/Si nanocables and the Si nanotubes can be controlled by adjusting the deposition time of the Si sheath and the morphologies of the ZnS template, respectively. Considering the large specific surface areas and stability, Si nanotubes were used as the SERS-active substrates for the highly sensitive detection of organic moleculars and effective photocatalyst for the degradation of organic dyes.

Acknowledgments

The authors would like to appreciate the financial supports from 973 Project (No. 2007CB936001, 2009CB623003), and the National Natural Science Foundation of China (NSFC Grants 21073212).

References

[1] Y. Myung, D. M. Jang, T. K. Sung et al., "Composition-tuned ZnO—CdSSe core—shell nanowire arrays," *ACS Nano*, vol. 4, no. 7, pp. 3789–3800, 2010.

[2] J. Xu, C. S. Lee, Y. B. Tang et al., "Large-scale synthesis and phase transformation of CuSe, $CuInSe_2$, and $CuInSe_2/CuInS_2$ core/shell nanowire bundles," *ACS Nano*, vol. 4, no. 4, pp. 1845–1850, 2010.

[3] L. Wang, J. Jie, C. Wu et al., "Coaxial ZnSe/Si nanocables with controlled p-type shell doping," *Nanotechnology*, vol. 21, no. 28, Article ID 285206, 2010.

[4] X. Fan, X. M. Meng, X. H. Zhang et al., "Formation and photoelectric properties of periodically twinned Znse/Sio nanocables," *Journal of Physical Chemistry C*, vol. 113, no. 3, pp. 834–838, 2009.

[5] M. W. Murphy, P. S. G. Kim, X. Zhou et al., "Biaxial ZnO-ZnS nanoribbon heterostructures," *Journal of Physical Chemistry C*, vol. 113, no. 12, pp. 4755–4757, 2009.

[6] Y. J. Hwang, A. Boukai, and P. Yang, "High density n-S/n-TiO core/shell nanowire arrays with enhanced photoactivit," *Nano Letters*, vol. 9, no. 1, pp. 410–415, 2009.

[7] N. S. Lewis, "Toward cost-effective solar energy use," *Science*, vol. 315, no. 5813, pp. 798–801, 2007.

[8] B. Tian, X. Zheng, T. J. Kempa et al., "Coaxial silicon nanowires as solar cells and nanoelectronic power sources," *Nature*, vol. 449, no. 7164, pp. 885–889, 2007.

[9] A. M. Morales and C. M. Lieber, "A laser ablation method for the synthesis of crystalline semiconductor nanowires," *Science*, vol. 279, no. 5348, pp. 208–211, 1998.

[10] Y. Wang, V. Schmidt, S. Senz, and U. Gösele, "Epitaxial growth of silicon nanowires using an aluminium catalyst," *Nature Nanotechnology*, vol. 1, no. 3, pp. 186–189, 2006.

[11] K. Peng, Y. Wu, H. Fang, X. Zhong, Y. Xu, and J. Zhu, "Uniform, axial-orientation alignment of one-dimensional single-crystal silicon nanostructure arrays," *Angewandte Chemie—International Edition*, vol. 44, no. 18, pp. 2737–2742, 2005.

[12] J. D. Holmes, K. P. Johnston, R. C. Doty, and B. A. Korgel, "Control of thickness and orientation of solution-grown silicon nanowires," *Science*, vol. 287, no. 5457, pp. 1471–1473, 2000.

[13] M. B. Ishai and F. Patolsky, "Shape-and dimension-controlled single-crystalline silicon and sige nanotubes: toward nanofluidic fet devices," *Journal of the American Chemical Society*, vol. 131, no. 10, pp. 3679–3689, 2009.

[14] N. J. Quitoriano, M. Belov, S. Evoy, and T. I. Kamins, "Single-crystal, Si nanotubes, and their mechanical resonant properties," *Nano Letters*, vol. 9, no. 4, pp. 1511–1516, 2009.

[15] J. Wang, X. J. Wang, Y. Jiao, Q. Li, M. W. Chu, and M. Malac, "From nanoparticle to nanocable: impact of size and geometrical constraints on the optical modes of Si/SiO_2 core/shell nanostructures," *Applied Physics Letters*, vol. 95, no. 13, Article ID 133102, 2009.

[16] M. L. Zhang, X. Fan, J. S. Jie, J. P. Hsu, and N. B. Wong, "Millimeter-long and uniform silicon nanocables," *Journal of Physical Chemistry C*, vol. 112, no. 41, pp. 15943–15947, 2008.

[17] J. Hu, Y. Bando, Z. Liu, T. Sekiguchi, D. Golberg, and J. Zhan, "Epitaxial heterostructures: side-to-side Si-Zns, Si-ZnSe biaxial nanowires, and sandwichlike Zns-Si-Zns triaxial nanowires," *Journal of the American Chemical Society*, vol. 125, no. 37, pp. 11306–11313, 2003.

[18] C. Wang, J. Wang, Q. Li, and G. C. Yi, "ZnSe-Si Bi-coaxial nanowire heterostructures," *Advanced Functional Materials*, vol. 15, no. 9, pp. 1471–1477, 2005.

[19] T. Ghoshal, S. Biswas, and S. Kar, "Synthesis of Ag/Si core/shell coaxial nanowire heterostructures by the vapor-liquid-solid technique," *Journal of Physical Chemistry C*, vol. 112, no. 51, pp. 20138–20142, 2008.

[20] Y. Xia, P. Yang, Y. Sun et al., "One-dimensional nanostructures: synthesis, characterization, and applications," *Advanced Materials*, vol. 15, no. 5, pp. 353–389, 2003.

[21] P. Yu, X. Zhang, D. Wang, L. Wang, and Y. Ma, "Shape-controlled synthesis of 3D hierarchical MnO_2 nanostructures for electrochemical supercapacitors," *Crystal Growth and Design*, vol. 9, no. 1, pp. 528–533, 2009.

[22] G. Q. Yuan, H. F. Jiang, C. Lin, and S. J. Liao, "Shape- and size-controlled electrochemical synthesis of cupric oxide nanocrystals," *Journal of Crystal Growth*, vol. 303, no. 2, pp. 400–406, 2007.

[23] N. Lin, J. Huang, P. R. Chang, D. P. Anderson, and J. H. Yu, "Preparation, modification, and application of starch nanocrystals in nanomaterials. A review," *Journal of Nanomaterials*, vol. 13, Article ID 573687, 2011.

[24] X. M. Meng, J. Liu, Y. Jiang et al., "Structure- and size-controlled ultrafine ZnS nanowires," *Chemical Physics Letters*, vol. 382, no. 3-4, pp. 434–438, 2003.

[25] Y. Jiang, X. M. Meng, J. Liu, Z. Y. Xie, C. S. Lee, and S. T. Lee, "Hydrogen-assisted thermal evaporation synthesis of ZnS nanoribbons on a large scale," *Advanced Materials*, vol. 15, no. 4, pp. 323–327, 2003.

[26] S. Nie and S. R. Emory, "Probing single molecules and single nanoparticles by surface-enhanced Raman scattering," *Science*, vol. 275, no. 5303, pp. 1102–1106, 1997.

[27] J. Theiss, P. Pavaskar, P. M. Echternach, R. E. Muller, and S. B. Cronin, "Plasmonic nanoparticle arrays with nanometer separation for high-performance SERS substrates," *Nano Letters*, vol. 10, no. 8, pp. 2749–2754, 2010.

[28] M. W. Shao, L. Lu, H. Wang et al., "An ultrasensitive method: surface-enhanced Raman scattering of Ag nanoparticles from β-silver vanadate and copper," *Chemical Communications*, no. 20, pp. 2310–2312, 2008.